The Canadian Mineralogist
Vol. 43, pp. 973-987 (2005)

TEM AND X-RAY STUDY OF SYNTACTIC INTERGROWTHS OF EPISTOLITE, MURMANITE AND SHKATULKALITE

PÈTER NÈMETH* AND GIOVANNI FERRARIS

Dipartimento di Scienze Mineralogiche e Petrologiche, Università di Torino, and Istituto di Geoscienze e Georisorse, CNR, Via Valperga Caluso, 35, I–10125, Torino, Italy

GYÖRGY RADNÓCZI

Research Institute for Technical Physics and Materials Science, Konkoly Thege Miklós út 29-33, H–1121 Budapest, Hungary

OLGA A. AGEEVA

Institute of Ore Deposits, Petrography, Mineralogy and Geochemistry, RAS, Staromonetny per., 35, RU–109017 Moscow, Russia

ABSTRACT

Selected-area electron diffraction (SAED) patterns obtained on samples of the heterophyllosilicates epistolite and murmanite from Mt. Malyi Punkaruaiv, Lovozero massif, in the Kola Peninsula of Russia, invariably show broad, streaked and split diffraction-spots and reveal oriented intergrowths (syntaxy) between the two minerals and of epistolite with minor shkatulkalite (likely a heterophyllosilicate as well). These results are confirmed by X-ray single-crystal and powder-diffraction data. We show that the syntaxy is favored by the presence in epistolite, murmanite and shkatulkalite of common supercells, which leads to a systematic overlap of diffraction spots belonging to different intergrown minerals. The structure determination of epistolite and murmanite by using "single-crystal" diffraction intensities contributed also by minor intergrown phases shows substantial residual peaks of electron density and some short bond-lengths. The difficulties encountered in properly refining the structures of the main phases are related to the unresolved contributions of the minor intergrown phases to the diffracted intensities. We suggest the ideal formulae $(Na,\square)_2\{(Na,Ti)_4[Nb_2(O,H_2O)_4Si_4O_{14}](OH,F)_2\}\bullet 2H_2O$ for epistolite and $(Na,\square)_2\{(Na,Ti)_4[Ti_2(O,H_2O)_4Si_4O_{14}](OH,F)_2\}\bullet 2H_2O$ for murmanite.

Keywords: epistolite, murmanite, shkatulkalite, heterophyllosilicates, titanosilicates, epitaxy, electron microscopy, crystal structure, mero-plesiotype series.

SOMMAIRE

Nous avons obtenu des spectres de diffraction d'électrons sur aire restreinte pour des échantillons des hétérophyllosilicates épistolite et murmanite provenant du mont Malyi Punkaruaiv, complexe alcalin de Lovozero, dans la péninsule de Kola en Russie; ils montrent dans tous les cas des taches de diffraction floues, etirées, et fendues, et révèlent des intercroissances orientées (syntaxie) entre les deux minéraux et de l'épistolite avec shkatulkalite (tout probablement aussi un hétérophyllosilicate) accessoire. Ces résultats sont confirmés par les données en diffraction X obtenues avec monocristaux et sur poudre. La syntaxie est favorisée par la présence d'épistolite, de murmanite et de shkatulkalite avec des surmailles communes, ce qui mène à une surimposition des taches de diffraction appartenant aux divers minéraux en intercroissance. La détermination de la structure de l'épistolite et de la murmanite au moyen d'intensités de diffraction à partir de "monocristaux" ayant des contributions attribuables aux quantités mineures des phases en intercroissance font preuve d'une densité résiduelle d'électrons substantielle, et des longueurs de liaisons anormalement courtes. Les difficultés rencontrées dans ces affinements de la structure des phases principales sont causées par les contributions non résolues aux intensités totales par les phases mineures en intercroissance. Nous proposons comme formules idéales $(Na,\square)_2\{(Na,Ti)_4[Nb_2(O,H_2O)_4Si_4O_{14}](OH,F)_2\}\bullet 2H_2O$ pour l'épistolite et $(Na,\square)_2\{(Na,Ti)_4[Ti_2(O,H_2O)_4Si_4O_{14}](OH,F)_2\}\bullet 2H_2O$ pour la murmanite.

(Traduit par la Rédaction)

Mots-clés: épistolite, murmanite, shkatulkalite, hétérophyllosilicates, titanosilicates, syntaxie, microscopie électronique, structure cristalline, série à caractère méro-plésiotype.

---

§ *Present address*: Departments of Geological Sciences & Chemistry/Biochemistry, Arizona State University, Tempe, Arizona 85287–1404, USA. *E-mail address*: peter.nemeth@asu.edu

INTRODUCTION

Epistolite, murmanite and presumably shkatulkalite are heterophyllosilicates whose structures are based on a *HOH* layer, where *H* is a phyllosilicate-like sheet of tetrahedra with inserted rows of 5- or 6-coordinated (Ti,Nb), and *O* is a sheet of octahedra, as defined by Ferraris *et al*. (1996). These minerals are members of the bafertisite mero-plesiotype series with general formula $A_2\{Y_4[Z_2(O')_{2+p}Si_4O_{14}](O'')_2\}W$ [Table 1; Ferraris 1997, Ferraris *et al*. 2001b; see Egorov-Tismenko & Sokolova (1990), for an earlier crystal-chemical analysis of some members of this series and quotation of Russian papers on the topic, and Ferraris & Gula (2005) for microporous properties]. In the formula, $[Z_2(O')_{2+p}Si_4O_{14}]^{n-}$ and $\{Y_4[Z_2(O')_{2+p}Si_4O_{14}](O'')_2\}^{m-}$ are complex anions representing the heteropolyhedral *H* sheet and the heterophyllosilicate *HOH* layer; *A* represents large interlayer cations; *W* represents other interlayer components, and *Y* are octahedral cations, respectively; O' (bonded to *Z* = Ti, Nb, Fe, Zr and not belonging to *O*) and O'' (belonging to *O*) are not bonded to Si and correspond to O, OH, F and H_2O. The value of *p* (0, 1, 2) depends on the coordination of *Z* and the

TABLE 1. MEMBERS OF THE MERO-PLESIOTYPE BAFERTISITE SERIES IN INCREASING ORDER OF THE CELL PARAMETER (*t*; EITHER *c* OR *a*) PERPENDICULAR TO THE STACK OF LAYERS

Name	Notes	Chemical formula	t [m]	Reference [l]
Murmanite	a	$(Na,\square)_2\{(Na,Ti)_4[Ti_2(O,H_2O)_4Si_4O_{14}](OH,F)_2\}\cdot 2H_2O$	11.70	This paper
Bafertisite	a	$Ba_2\{(Fe,Mn)_4[Ti_2O_2(O,OH)_2Si_4O_{14}](O,OH)_2\}$	11.73	Guan *et al*. (1963)
Hejtmanite	a	$Ba_2\{(Mn,Fe)_4[Ti_2(O,OH)_4Si_4O_{14}](OH,F)_2\}$	11.77	Rastsvetaeva *et al*. (1991)
Epistolite	b	$(Na,\square)_2\{(Na,Ti)_4[Nb_2(O,H_2O)_4Si_4O_{14}](OH,F)_2\}\cdot 2H_2O$	12.14	This paper
Vuonnemite	b	$Na_8\{(Na,Ti)_4[Nb_2O_2Si_4O_{14}](O,OH,F)_2\}(PO_4)_2$	14.45	Ercit *et al*. (1998)
Lomonosovite	a, n	$Na_8\{(Na,Ti)_4[Ti_2O_2Si_4O_{14}](O,OH)_2\}(PO_4)_2$	14.50	Belov *et al*. (1978)
Yoshimuraite	a, c	$Ba_4\{Mn_4[Ti_2O_2Si_4O_{14}](OH)_2\}(PO_4)_2$	14.75	McDonald *et al*. (2000)
Innelite	b, c	$(Ba,K)_2Ba_2\{(Na,Ca,Ti)_4[Ti_2O_2Si_4O_{14}]O_2\}(SO_4)_2$	14.76	Chernov *et al*. (1971)
Bussenite	a	$Ba_4Na_2\{(Na,Fe,Mn)_2[Ti_2O_2Si_4O_{14}](OH)_2\}(CO_3)_2F_2\cdot 2H_2O$	16.25	Zhou *et al*. (2002)
Seidozerite	b, g, i	$Na_2\{(Na,Mn,Ti)_4[(Zr,Ti)_2O_2Si_4O_{14}]F_2\}$	18.20	Pushcharovsky *et al*. (2002)
Lamprophyllite	b, c	$(Sr,Ba)_2\{(Na,Ti)_4[Ti_2O_2Si_4O_{14}](OH,F)_2\}$	19.49	Rastsvetaeva *et al*. (1990)
Nabalamprophyllite	b, c	$Ba(Na,Ba)\{(Na,Ti)_4[Ti_2O_2Si_4O_{14}](OH,F)_2\}$	19.74	Rastsvetaeva & Chukanov (1999)
Barytolamprophyllite	b, c	$(Ba,Na)_2\{(Na,Ti)_4[Ti_2O_2Si_4O_{14}](OH,F)_2\}$	19.83	Pen *et al*. (1984)
Orthoericssonite	b, c	$Ba_2\{Mn_4[Fe_2O_2Si_4O_{14}](OH)_2\}$	20.23	Matsubara (1980)
Quadruphite	a	$Na_{13}Ca\{(Ti,Na,Mg)_4[Ti_2O_2Si_4O_{14}]O_2\}(PO_4)_4F_2$	20.36	Sokolova & Hawthorne (2001)
Ericssonite	e	$Ba_2\{Mn_4[Fe_2O_2Si_4O_{14}](OH)_2\}$	20.42	Moore (1971)
Surkhobite	a, i	$(Ca,Na,Ba,K)_2\{(Fe,Mn)_4[Ti_2O_2Si_4O_{14}](F,O,OH)_3\}$	20.79	Rozenberg *et al*. (2003)
Jinshajiangite	e, p	$(Na,Ca)(Ba,K)\{(Fe,Mn)_4[(Ti,Nb)_2O_2Si_4O_{14}](F,O)_2\}$	20.82	Hong & Fu (1982)
Perraultite	a, i	$(Na,Ca)(Ba,K)\{(Mn,Fe)_4[(Ti,Nb)_2O_2Si_4O_{14}](OH,F)_2\}$	20.84	Yamnova *et al*. (1998)
Delindeite	b	$Ba_2\{(Na,Ti,\square)_4[Ti_2(O,OH)_4Si_4O_{14}](H_2O,OH)_2\}$	21.51	Ferraris *et al*. (2001b)
Polyphite	a	$Na_{14}(Ca,Mn,Mg)_5\{(Ti,Mn,Mg)_4[Ti_2O_2Si_4O_{14}]F_2\}(PO_4)_6F_4$	26.56	Sokolova *et al*. (1987)
M55C	e	$Na_8\{(Na,Ti)_4[Ti_2O_2Si_4O_{14}](O,F)_2\}(PO_4)_2$?	28.1	Nèmeth (2004)
Shkatulkalite	e	$\{(Na,Mn,Ca,\square)_4[(Nb,Ti)_2(H_2O)_2Si_4O_{14}](OH,H_2O,F)_2\}\cdot 2(H_2O,\square)$	31.1	Men'shikov *et al*. (1996)
M55A	e	$Ba(Na,\square)_5\{(Na_3Ti)[(Ti,Nb)_2O_2Si_4O_{14}](F,OH,O)_2\}\cdot(PO_4)_2\cdot 4H_2O$	38.11	Nèmeth (2004)[f], Khomyakov (1995)
Sobolevite	a	$Na_{12}CaMg\{(Ti,Na,Mg)_4[Ti_2O_2Si_4O_{14}]O_2\}(PO_4)_4F_2$	40.62	Sokolova *et al*. (1988)
M55B	e	$\{(Na,K,Ba,\square)_4[(Ti,Nb)_2(H_2O,OH)_2Si_4O_{14}](F,H_2O,\square)_2\}$	43.01	Nèmeth (2004)
Bornemanite	a, i	$BaNa_3\{(Na,Ti,Mn)_4[(Ti,Nb)_2O_2Si_4O_{14}](F,OH)_2\}PO_4$	47.95	Ferraris *et al*. (2001a)
M73	a, d	$(Ba,Na)_2\{(Na,Ti,Mn)_4[(Ti,Nb)_2(OH)_3Si_4O_{14}](OH,O,F)_2\}\cdot 3H_2O$	48.02	Nèmeth (2004)[f], Khomyakov (1995)
M72	a, d, h	$BaNa\{(Na,Ti)_4[(Ti,Nb)_2(OH,O)_3Si_4O_{14}](OH,F)_2\}\cdot 3H_2O$	50.94	Nèmeth (2004)[f], Khomyakov (1995)

The content of the heteropolyhedral *H* sheet is shown in square brackets, and that of the *HOH* layer is within braces; the composition of the interlayer is shown outside the braces. The table is derived, with additions and modifications, from Ferraris *et al*. (2001b, 2004). Notes: a) $(HOH)_B$ layer. b) $(HOH)_V$ layer. c) *Z* cation in coordination 5. d) *Z* cation in coordinations 5 and 6. e) Structure unknown; the inclusion in this table is based mainly on chemical and crystal data. f) Crystallographic data. g) Grenmarite (Bellezza *et al*. 2004) is a new species that differs from seidozerite in having Zr dominant also in one site of the *O* sheet. Actually, seidozerite is included in this Table more for historical [see the first introduction of this series by Egorov-Tismenko & Sokolova (1990)] than structural reasons; in fact, sharing of edges between adjacent *HOH* layers and the consequent lack of a real interlayer space suggest the inclusion of seidozerite in the götzenite – rosenbuschite – seidozerite family (*cf*. Christiansen *et al*. 2003, Bellezza *et al*. 2004). h) Approved as mineral species: IMA No 2003–044 (Burke & Ferraris 2004). i) Two octahedra of *Z* cations share either a corner or an edge. l) Reference to the most recent paper describing the structure, where known, otherwise to the paper describing the species. m) The unit cells given by authors have been converted to reduced unit-cells, where applicable. n) "Betalomonosovite" is a discredited species with a composition close to that of lomonosovite; its crystal structure was determined by Rastsvetaeva (1998) (*a* 5.326, *b* 14.184, *c* 14.47 Å, α 102.2, β 95.5, γ 90.17°; $P\bar{1}$). p) The IR spectra (N.V. Chukanov, pers. commun.), cell parameters and composition suggest that jinshajiangite has the same structure of perraultite, thus corresponding to the Fe-dominant analogue of the latter mineral.

linkage of its polyhedron. This series is considered merotypic because the *HOH* module is invariably present in the crystal structure of all members, whereas a second module, namely the interlayer content, is particular to each member. [Note that according to Makovicky (1997), in a merotype series, whereas one building module is kept constant, a second (third, *etc*.) module is particular to each member.] However, the series also has a plesiotype character because the nature and coordination number of the *Z* and *Y* cations and the linkage between the *H* and *O* sheets are not constant. [A series is said to be plesiotype if all members share modules that, however, may still slightly differ in chemistry and configuration. For several examples, see Ferraris *et al*. (2004).] In fact, as recently discussed by Sokolova & Hawthorne (2004), by comparing the crystal structures of epistolite and murmanite, the two *H* sheets sandwiching an *O* sheet may or may not show a relative shift (see also Christiansen *et al*. 1999). The two kinds of *HOH* layer occurring in vuonnemite, $(HOH)_V$, and in bafertisite, $(HOH)_B$, are here taken as typical examples; their occurrence is explained in footnotes *a* and *b* to Table 1.

As part of a research program aiming to better characterize members of the mero-plesiotype bafertisite series (Table 1), we report in this paper results obtained by transmission electron microscopy (TEM) and single-crystal X-ray diffraction (SXD) that show syntactic intergrowths between murmanite and epistolite and of the latter with shkatulkalite as well. The origin of the structural disorder observed in our samples and, presumably, of that reported in previous papers on epistolite (Sokolova & Hawthorne 2004) and murmanite (Khalilov 1989, Rastsvetaeva & Andrianov 1986) is discussed in light of this syntaxy.

Review of Previous Results

The chemically and structurally similar hyperalkaline minerals epistolite and murmanite are hydrous secondary phases, which, in the epithermal and supergene processes, replace the primary minerals vuonnemite and lomonosovite (Table 1), respectively, *via* solid-state reactions. [Note that the wording "solid-state transformation" widely used in this paper does not exclude the intervention of local dissolution and recrystallization, a matter widely debated (*cf*. Putnis 2002). With its use, we intend to emphasize that primary and secondary phases differ mainly in the interlayer contents in a way at least formally amenable to leaching or exchange processes.] Khomyakov (1995) called this type of secondary phases transformation minerals [see also Pekov (2000) and Pekov & Chukanov (2005)]. Epistolite has been reported in the alkaline complexes of Ilímaussaq (South Greenland; Bøggild 1901) and Lovozero (Kola Peninsula, Russia; Semenov *et al*. 1962). It forms creamy to yellow plates up to a few cm wide and half a cm in thickness and consist of very thin lamellae. Murmanite was first reported from Lovozero by Ramsay (1890) and then characterized by Gutkova (1930); later it was found also at Ilímaussaq (Buchwald & Sørensen 1961). Murmanite forms lamellar crystals lilac to pink in color up to several centimeters across. Shkatulkalite occurs at Lovozero with vuonnemite and epistolite; in some cases, it forms a pseudomorph after vuonnemite (Men'shikov *et al*. 1996, Pekov 2000). Presumably, shkatulkalite also is a secondary phase derived from one of the primary phases mentioned (*cf*. pseudomorphs); however, the lack of a crystal-structure determination makes it difficult to discuss further the genesis of shkatulkalite. Its inclusion among heterophyllosilicates (Table 1) may be considered questionable, as it is based mainly on chemical and crystallographic data and paragenesis.

The mechanism of formation of the secondary phases, which preserve in their crystal structure the *HOH* layer of the parent structures and modify the interlayer composition only ["inheritance principle" of Khomyakov (1995)], and their pseudosymmetry, favor various kinds of disorder and intergrowths, as discussed below. These phenomena render single-crystal X-ray studies problematic; in particular, the presence in the diffraction patterns of broad, streaked, split and even extra reflections has been reported (Khalilov *et al*. 1965, Khalilov 1989, Rastsvetaeva & Andrianov 1986, Sokolova & Hawthorne 2004). On the basis of results of chemical analyses, Khalilov *et al*. (1965) inferred the presence in murmanite of secondary phases derived from the parent phase lomonosovite. The occurrence of extra diffraction-spots was interpreted by Karup-Møller (1986b) as due to unidentified submicroscopic phases in epistolite and led Rastsvetaeva & Andrianov (1986) to assign a multiple cell to murmanite. Semenov *et al*. (1962) introduced the term "metamurmanite" to refer to an intermediate phase that appears during the transformation from lomonosovite to murmanite. Ferraris & Nèmeth (2003) proposed an occurrence of twinning by reticular pseudomerohedry.

While this research was in progress (Ferraris & Nèmeth 2003), Sokolova & Hawthorne (2004) published a structure with positional disorder for epistolite. Their single-crystal X-ray refinement of the structure of a crystal from the original locality at Ilímaussaq (*a* 7.460, *b* 7.170, *c* 12.041 Å, α 103.63, β 96.01, γ 89.98°; space group $P\bar{1}$) converged to R = 9.8% and showed some unusually short bond-lengths (see below) and substantial residual electron-density close to the Nb and Si sites. These residues correspond to about 10% of either Nb or Si, and are attributed by the authors to the unidentified submicroscopic phase mentioned by Karup-Møller (1986b). Similar residual peaks close to the Nb and Si sites occur in the structure of murmanite first refined in *P*1 by Khalilov *et al*. (1965) to R_{h0l} = 14.5% and R_{hk0} = 18.2% (two-dimensional data only) and later (Khalilov 1989) to R = 7.5% using three-dimensional data. Rastsvetaeva & Andrianov (1986)

redetermined the crystal structure of murmanite in *P*1 (*a* 8.700, *b* 8.728, *c* 11.688 Å, α 94.31, β 98.62, γ 105.62°; R = 9.1%) starting from a quadruple triclinic *C*-centered cell with doubled *a* and *b* parameters.

Khalilov (1989), Egorov-Tismenko & Sokolova (1990) and Ercit *et al.* (1998) considered epistolite and murmanite to be isostructural; Sokolova & Hawthorne (2004) showed that these two minerals are not isostructural and have topologically distinct *HOH* layers. In fact, according to our terminology, epistolite and murmanite are based on the $(HOH)_V$ and $(HOH)_B$ layers mentioned above.

Experimental Results

The samples of epistolite and murmanite used for this work were collected from a microcline–sodalite pegmatite within foyaite at Mt. Malyi Punkaruaiv in the Lovozero peralkaline massif. White laths of epistolite 0.2–0.5 cm across, and violet laths of murmanite 0.5–4.0 cm across replacing vuonnemite and lomonosovite, respectively, are associated mainly with ussingite, sodalite, analcime, arfvedsonite, mangan-neptunite, belovite, catapleiite, Ca-rich sérandite, gerasimovskite, chkalovite, loparite, sphalerite, and galena.

Samples of epistolite and murmanite were investigated by transmission electron microscopy (TEM), powder and single-crystal X-ray diffraction, and their composition was established by electron-microprobe analysis. The following instruments were used: Philips CM12 transmission electron microscope (LaB_6 filament, operated at 120 kV; University of Torino); Technoorg–Linda ion-beam miller (Research Institute for Technical Physics and Materials Science, Budapest); Siemens *P*4 X-ray single-crystal diffractometer (graphite monochromator, Mo*K*α radiation; University of Torino); electron microprobe (ARL–SEMQ in WDS mode, 15kV, 20 nA, beam diameter 20 μm; University of Modena and Reggio Emilia); Philips X'Pert X-ray powder diffractometer (Cu*K*α radiation, graphite monochromator; University of Milano and Institute of Chemistry of the Chemical Research Center HAS, Budapest).

Chemical composition

On the basis of 4 (Si + Al) atoms per formula unit, according to the general formula for the bafertisite series shown above ($p = 2$), the following crystal-chemical formula is obtained for epistolite from the analytical data of Table 2, after subtraction of phosphorus as vuonnemite with ideal composition $Na_8\{(Na_3Ti[Nb_2O_2Si_4O_{14}](OH)O\}(PO_4)_2$: $Na_{0.25}\{(Na_{2.77}Ti_{0.60}Ca_{0.40}Fe^{2+}_{0.01}Mn_{0.14}K_{0.09})_{\Sigma 4}\ [(Nb_{1.50}Ti_{0.50})_{\Sigma 2}((OH)_{2.08}(H_2O)_{1.92})_{\Sigma 4}(Si_{3.97}Al_{0.03})_{\Sigma 4}O_{14}]((OH)_{1.20}F_{0.80})_{\Sigma 2}\}\bullet 2.75H_2O$.

Applying the same procedure to data in Table 2, the following result was obtained for murmanite, after subtraction of phosphorus as lomonosovite with ideal formula $(Na_8\{(Na_{2.5}Ti_{1.5}[Ti_2O_2Si_4O_{14}](OH_{1.5}O_{0.5})\}(PO_4)_2$: $Na_{0.44}\{(Na_{1.40}Ti_{1.55}Ca_{0.34}Mn_{0.35}Fe^{2+}_{0.18}Mg_{0.12}K_{0.06})_{\Sigma 4}\ [(Ti_{1.30}Nb_{0.50}Zr_{0.20})_{\Sigma 2}(O_2(H_2O)_{1.43}(OH)_{0.57})_{\Sigma 4}(Si_{3.99}Al_{0.01})_{\Sigma 4}O_{14}]((OH)_{1.70}F_{0.30})_{\Sigma 2}\}\bullet 3.36H_2O$.

TEM observations

A study by TEM reveals that our samples of epistolite and murmanite consist of very thin and roughly equidimensional lamellae resulting from a perfect {001} cleavage. Observations along directions not perpendicular to (001) were acquired from samples prepared by ion-beam thinning. In general, the quality of the selected-area electron-diffraction (SAED) patterns is poor because the material is poorly crystalline and deteriorates quickly under the electron beam.

The SAED pattern shown in Figure 1 was obtained with the electron beam incident along [110] of a sample of epistolite (*e*); it allows detection of an oriented intergrowth (*i.e.*, syntaxy; Ungemach 1935) of the matrix with murmanite (*m*) and shkatulkalite (*s*). In Figure 1, each diffraction spot from epistolite overlaps with one of murmanite according to systematic rules discussed below. In this SAED, the overlap is almost perfect because epistolite and murmanite have close values of d_{001} (epistolite 11.7 Å, murmanite 11.6 Å) and $d_{\bar{1}10}$ (4.3 Å in both cases), and of the angle between [001]* and [$\bar{1}$10]* (86.1° in epistolite and 86.0° in murmanite). Thus, the syntaxy between epistolite and murmanite is discernible only by a broadening of the spots due, among other reasons, to some deviation from an exact overlap of the contributions diffracted by different phases. On the other hand, a clear identification of shkatulkalite

TABLE 2. CHEMICAL COMPOSITION OF EPISTOLITE AND MURMANITE

	Epistolite		Murmanite		Standards
	Average[1]	Range	Average[2]	Range	
Na_2O wt%	12.81	12.03 - 13.94	8.51	7.09 - 9.87	Albite
K_2O	0.52	0.39 - 0.64	0.32	0.31 - 0.34	Microcline
CaO	2.49	2.05 - 2.76	2.29	2.16 - 2.45	Anorthite
MgO	0.01	0.00 - 0.02	0.63	0.61 - 0.65	Olivine
FeO	0.10	0.07 - 0.15	1.56	1.50 - 1.64	Ilmenite
MnO	1.19	1.11 - 1.25	3.05	2.98 - 3.06	Fayalite[8]
Al_2O_3	0.20	0.15 - 0.25	0.08	0.06 - 0.10	Microcline
SiO_2	30.27	29.65 - 31.30	30.00	29.03 - 31.15	Microcline
TiO_2	11.13	10.21 - 12.13	28.57	26.88 - 29.93	Ilmenite
Nb_2O_5	25.62	24.49 - 27.09	8.06	6.99 - 8.66	Metallic Nb
ZrO_2	0.01	0.00 - 0.04	2.99	2.77 - 3.27	Metallic Zr
P_2O_5*	0.53	0.33 - 0.74	0.63	0.57 - 0.68	Apatite
F	1.87	1.44 - 2.65	0.72	0.45 - 0.82	Fluorite
$-O = F_2$	0.79		0.30		
H_2O[3]	14.04		12.89		
Total	100.00		100.00		

[1] Five point-analyses made with an electron microprobe.
[2] Four point-analyses made with an electron microprobe.
[3] H_2O calculated by difference. [8] Manganese- and magnesium-bearing fayalite.

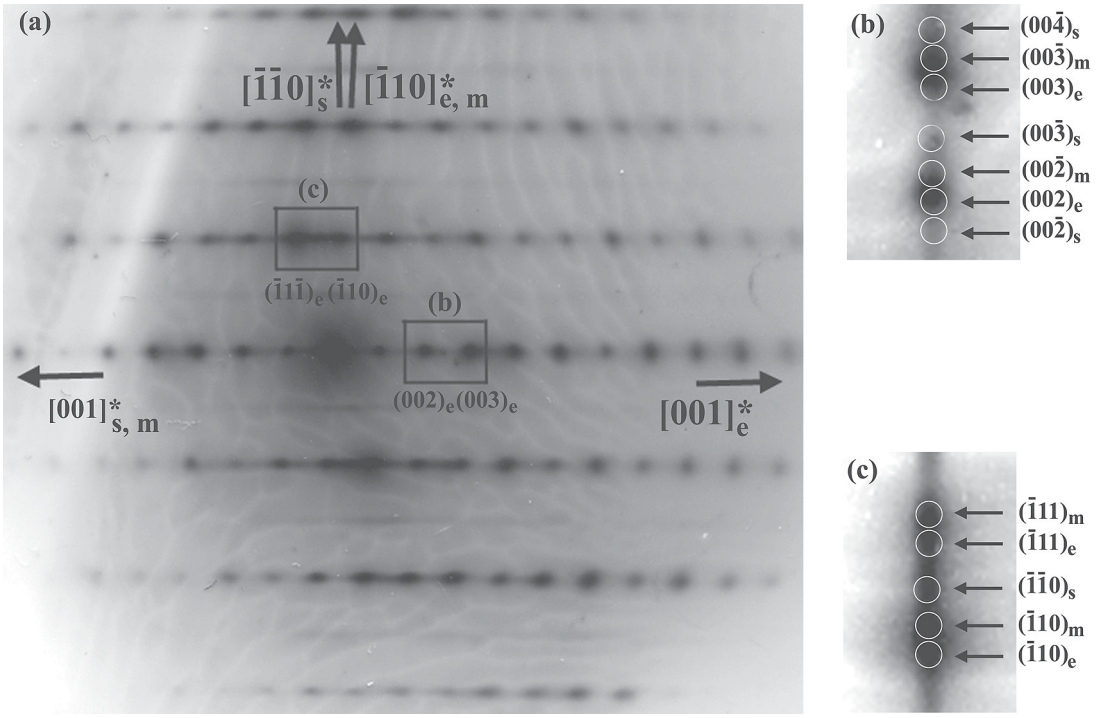

FIG. 1. SAED pattern of epistolite taken along [110]. In (a), the arrows indicate the directions of rows belonging to the matrix epistolite (e), the minor intergrown phases shkatulkalite (s) and murmanite (m). The insets (b) and (c) show examples of (partial) overlap between indexed spots diffracted by different phases. Very weak and diffuse rows parallel to [001]* might suggest doubling of the *a* and *b* parameters of epistolite. The absence of odd values of the *l* index of shkatulkalite is discussed in the text.

is possible; even if this mineral and epistolite have in common the [001]* direction, their *c** parameters differ substantially (0.0645 Å^{-1} for shkatulkalite and 0.0854 Å^{-1} for epistolite). [Note that according to the value of the *c* parameter (31.1 Å) reported by Men'shikov *et al.* (1996), the reflections with $l = 2n + 1$ are absent in the electron-diffraction patterns of shkatulkalite; thus, a halved *c* parameter can be used. A half *c* would match the powder-diffraction data published by the same authors as well. Thus, without losing generality in the discussion involving shkatulkalite, *c* = 15.55 Å is here used for this mineral.] Consequently, non-overlapping spots of shkatulkalite appear (Figs. 1a, b, c), particularly along the common [001]* direction. Finally, the very weak and diffuse rows that alternate with the strong ones along $[1\bar{1}0]^*$ (Fig. 1a) might suggest doubling of the *a* and *b* parameters of epistolite, as found by Rastsvetaeva & Andrianov (1986) for murmanite.

The SAED pattern shown in Figure 2 is obtained with the beam oriented along the [112] direction of an epistolite matrix. Even if the spots contributed by epistolite, murmanite and shkatulkalite apparently form a unique lattice net, the systematic overlap (see below) is such that 50% of the spots are contributed by shkatulkalite and murmanite together, but not by epistolite. The two overlapping phases have close values of *a** (0.1833 Å^{-1} for shkatulkalite and 0.1874 Å^{-1} for murmanite), *b** (0.1393 Å^{-1} for shkatulkalite and 0.1416 Å^{-1} for murmanite) and β* (90.0° for shkatulkalite and 89.5° for murmanite). The insets (b) and (c) in Figure 2 illustrate the degree of overlap between some spots of shkatulkalite and murmanite. A dark-field image (Fig. 2d) obtained from the almost overlapped spots $(3\bar{2}0)_m$ and $(320)_s$ shows curved domains with an average size of 20–30 nm. According to other unreported but similar images, this is the typical size of the domains belonging to only one intergrown phase.

The SAED pattern of murmanite along [010] (Fig. 3) shows syntaxy of this phase with epistolite. Owing to the small (2.04°) but significant difference between the β* angles of epistolite (84.11°) and murmanite (82.07°), the divergence between the rows belonging to the two phases in some directions is such that overlap does not occur (Figs. 3b, c). A HRTEM image (Fig. 3d) reveals overlapped fringes of murmanite and epistolite (d_{001} = 11.6 Å) and a large area of fringes with 23.2 Å

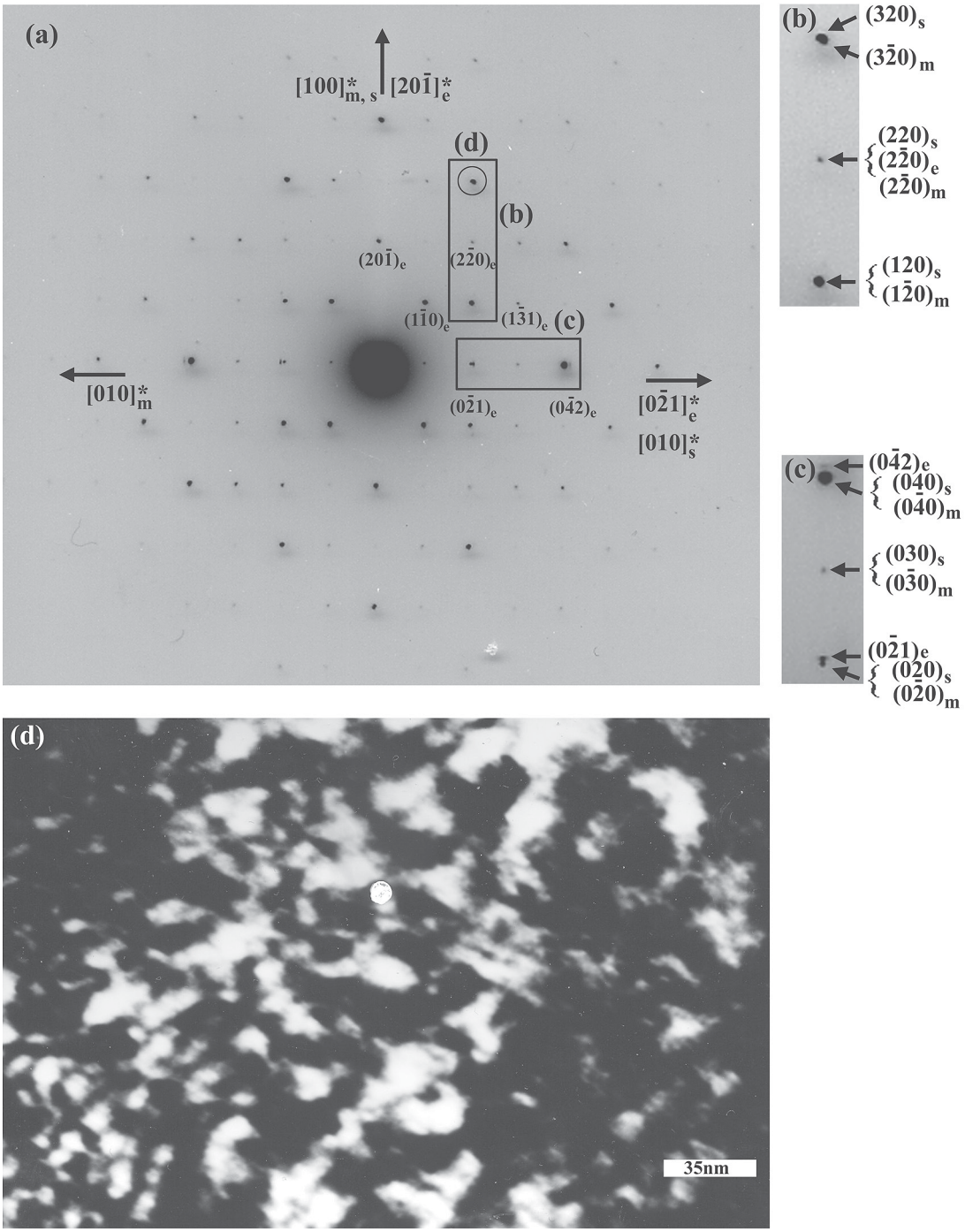

FIG. 2. SAED pattern of epistolite taken along [112]; arrows and insets as in Figure 1. The dark field image (d) has been obtained from the circled (d) spot shown in (a). In this spot, $(3\bar{2}0)_m$ and $(320)_s$ nearly overlap.

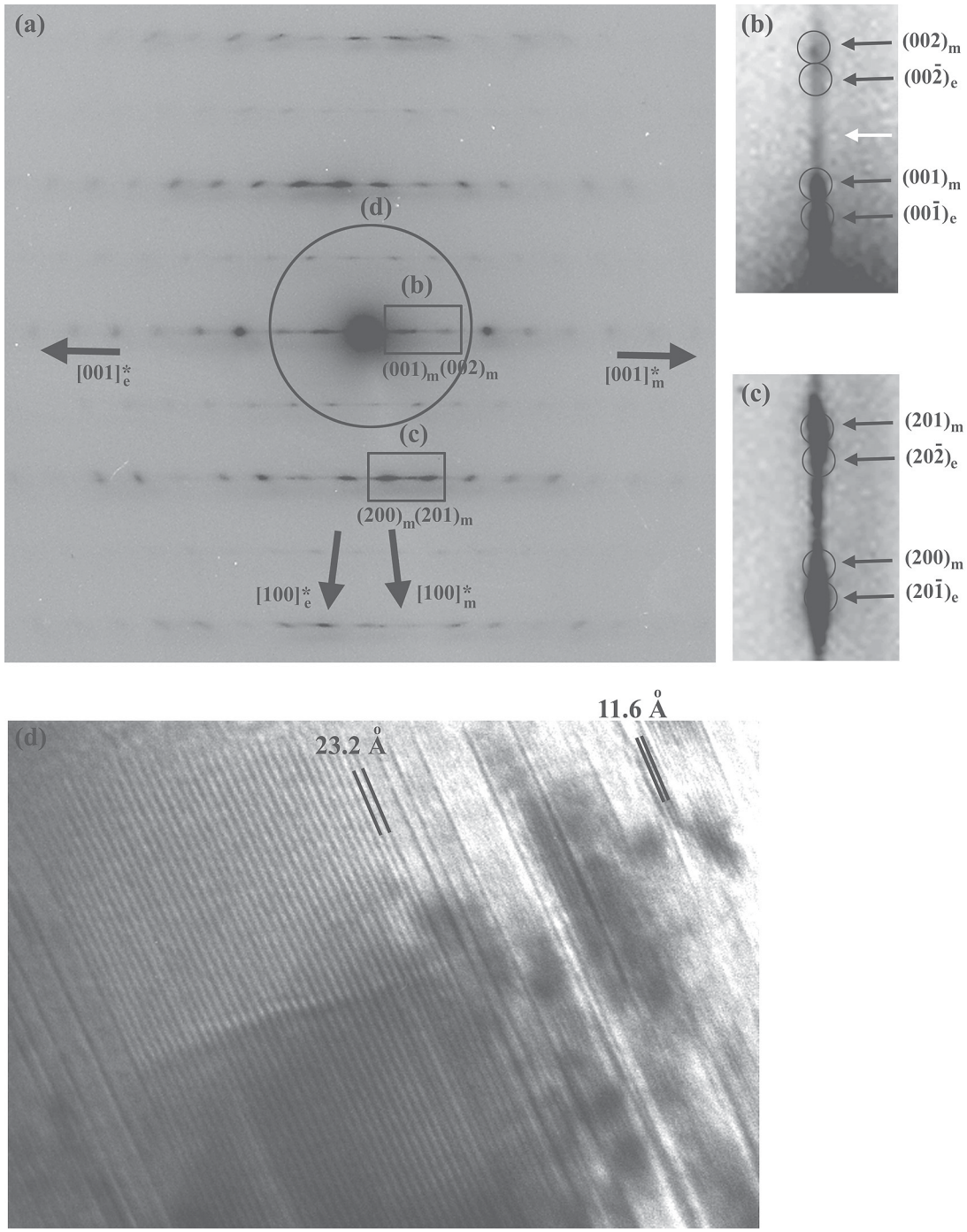

FIG. 3. SAED pattern of murmanite taken along [010]. Arrows and insets as in Figure 1; the white arrow in inset (b) shows a spot due to a possible doubling of the *c* parameter. The HRTEM image (d) has been obtained from the circled set of spots shown in (a); areas with 001 fringes (11.6 Å) due to murmanite (m) and epistolite (e) (or both), and double-width fringes (23.2 Å) related to doubling of the *c* parameter are present.

periodicity. The latter suggest doubling of the *c* parameter, in agreement with the occurrence of spots like that indicated by the white arrow in Figure 3b.

The doubling of cell parameters mentioned in reference to Figures 1 and 3 are not confirmed by the X-ray single-crystal study (see below); the weak spots suggest that this could be due both to the interaction of intergrown phases and to structural features present only locally in the small volumes intersected by the electron beam in a TEM observation.

Single-crystal X-ray diffractometry

Single-crystal X-ray-diffraction patterns were collected on poor crystals of epistolite and murmanite. Broad, streaked, split and extra spots were observed and interpreted (see discussion for TEM results) as due to oriented intergrowths of different phases and to disorder, for example involving the rotation of lamellae due to the easy {001} cleavage. The doubling of the *a* and *b* parameters observed by Rastsvetaeva & Andrianov (1986) for murmanite was not detected, nor was that of *c* discussed above in connection with Figure 3. As for the TEM data, in the X-ray single-crystal patterns, the contributions of the intergrown phases are not well separated from that of the matrix, either for epistolite or murmanite. Consequently, it has not been possible to obtain sets of diffraction data belonging to one single mineral phase only. The same problems with overlapping spots would be introduced by the occurrence of the type of twinning discussed below; we did not detect twinning, but its presence cannot be excluded.

The unit-cell parameters of epistolite and murmanite (Table 3) were obtained by least-squares refinement of angular values of selected reflections.

X-ray powder diffractometry

The X-ray powder-diffraction profiles of epistolite and murmanite are presented superimposed in Figure 4; they visually show the presence of the intergrown phases mentioned above plus others. More precisely, the pattern of epistolite contains also major shkatulkalite and minor vuonnemite; that of murmanite contains a phase characterized by an interplanar equidistance of 13.5 Å and called "metamurmanite" by Semenov *et*

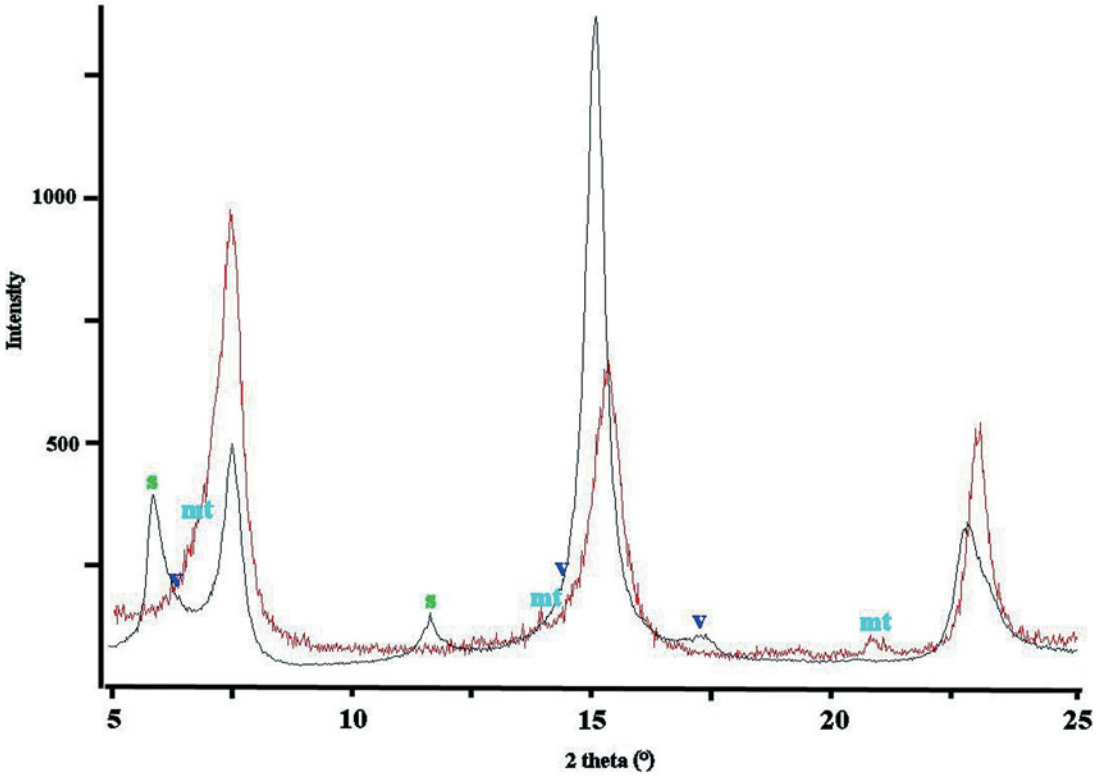

FIG. 4. Superimposed profiles of X-ray powder patterns of epistolite (black) and murmanite (red). The positions of the most intense peaks of shkatulkalite (s) and vuonnemite (v), present in the pattern of epistolite, and of "metamurmanite" (mt), present in the pattern of murmanite, are shown.

al. (1962). The peaks of epistolite and murmanite are almost exactly overlapped because these two heterophyllosilicates have very close unit-cell parameters (Table 3). Concerning the peaks due to the main phases, the present patterns do not differ substantially from those reported in literature for epistolite (Karup-Møller 1986b) and murmanite (Karup-Møller 1986a, Rastsvetaeva & Andrianov 1986).

Discussion

Reality and artifacts in the structures

Our attempts to refine the crystal structures of epistolite and murmanite led to the same kind of observations reported, to a different extent, in papers quoted above: (i) large residues occur in the difference electron-density maps, particularly close to the cations of the *H* sheet; (ii) anisotropic refinement is possible only for a limited number of atoms, at variance with the fully anisotropic refinement obtained by Sokolova & Hawthorne (2004) for epistolite; (iii) some unusually short bond-lengths are obtained (see below); (iv) convergence is reached at high R values. More precisely, in space group $P\bar{1}$, we have obtained R = 13.6% for epistolite and R = 6.2% for murmanite, to be compared with R = 9.8% and R = 7.5% published by Sokolova & Hawthorne (2004) and Khalilov (1989) for the two minerals, respectively. In both cases, our refinements in the space group *P*1 are not better than in $P\bar{1}$; thus, $P\bar{1}$ is preferred for both minerals. Our values of the atom coordinates do not differ substantially from those published by Sokolova & Hawthorne (2004) for epistolite and by Khalilov (1989) for murmanite. Consequently, taking into account that the main purpose of this paper is to correlate TEM observations with obstacles to properly refine the structures of epistolite and murmanite, tables of atom positions and bond lengths are not reported; the atom labeling used by Sokolova & Hawthorne (2004) is adopted.

The unusually short bond-lengths mentioned above occur in the *H* sheets of both epistolite and murmanite.

TABLE 3. X-RAY SINGLE-CRYSTAL DIFFRACTOMETRY: MISCELLANEOUS DATA FOR EPISTOLITE AND MURMANITE

	Epistolite	Murmanite		Epistolite	Murmanite
a (Å)	5.455(3)	5.387(3)	Crystal size	0.42 × 0.31	0.25 × 0.24
b (Å)	7.16(1)	7.079(6)	(mm)	× 0.06	× 0.07
c (Å)	12.14(1)	11.74(3)	Scan mode	2θ	2θ
α (°)	104.01(9)	93.80(4)	2θ range (°)	49.97	49.99
β (°)	95.89(7)	97.93(8)	Range of indices	±6 ±8 ±14	±6 ±8 ±13
γ (°)	90.03(9)	90.00(7)	R(int)	0.04(3)	0.05(6)
V (Å^3)	457.4(5)	441.67(5)	Collected refl.	3244	3120
Space group	$P\bar{1}$	$P\bar{1}$	Independent refl.	1622	1560
			$\|F_o\| > 4\sigma(\|F_o\|)$	1530	1343

We have found *M*(1)–O(9) (Fig. 5) to be equal to 1.79 and 1.83 Å for epistolite and murmanite, respectively; these values are comparable with the corresponding ones, 1.768 and 1.82 Å, published for epistolite (Sokolova & Hawthorne 2004) and murmanite (Khalilov 1989), respectively. According to the values of the ionic radii for 4-coordinated O^{2-} (1.38 Å) and octahedral Ti^{4+} (0.605 Å) and Nb^{5+} (0.64 Å) (Shannon 1976), Ti–O = 1.985 Å and Nb–O = 2.020 Å are expected. On the other hand, if the short *M*(1)–O(9) distance is excluded, the average value of the remaining (Ti,Nb)–O bonds is close to 2.0 Å both in our results and in those published for epistolite (Sokolova & Hawthorne 2004) and murmanite (Khalilov 1989).

To easily compare the two structures, they are referred to the same origin, fixed at the position of the Ti atom occurring in the *O* sheet; this position corresponds to a center of symmetry in epistolite, but not in murmanite (Fig. 5). As mentioned at the beginning of this paper, Sokolova & Hawthorne (2004) pointed out that the two structures are not isostructural: according to the labeling we introduce here, whereas epistolite contains the vuonnemite-type $(HOH)_V$ layer, murmanite contains instead the bafertisite-type $(HOH)_B$ layer. In principle, other than minor changes in the *O* sheet, one structure can be obtained from the other by exchanging the position of the M(1) octahedron (Fig. 5) with that of a silicon tetrahedron in one of the two *H* sheets belonging to the same *HOH* layer. Figure 6 shows the two structures overlapped according to the orientation of their intergrowths obtained from the SAED patterns of Figures 1, 2 and 3. One can see that the major difference between the overlapped structures is a relative shift of one out of two *H* sheets belonging to the same *HOH* layer; the rest of the two structures, in contrast, roughly coincides. A "computational transformation" of one structure into the other can be realized starting from the atom positions of one structure to refine the diffraction data of the other. Slowly, but definitely, the structure to which the diffraction data belong emerges. If, instead, diffraction data contributed by different intergrown phases are refined, the resulting image corresponds to the structure of the principal phase (*e.g.*, epistolite) plus a subordinate image of the intergrown phase (*e.g.*, murmanite). Actually, in our case, the results of the refinement are further complicated by the presence of other phases, among which shkatulkalite in epistolite and "metamurmanite" in murmanite. Finally, the presence of some twinning, for reasons discussed below, and of different polytypes cannot be excluded; polytypism has been found for other members of the series like ericssonite, lamprophyllite (Ferraris *et al*. 2004), M72 and M73 (Table 1; Nèmeth 2004). The weighted overlap of different structures affects the positions of the maxima in a map of electron density, *i.e.*, the positions of the atoms. Consequently, unusual bond-lengths may appear, such as the short M(1)–O(9) mentioned above.

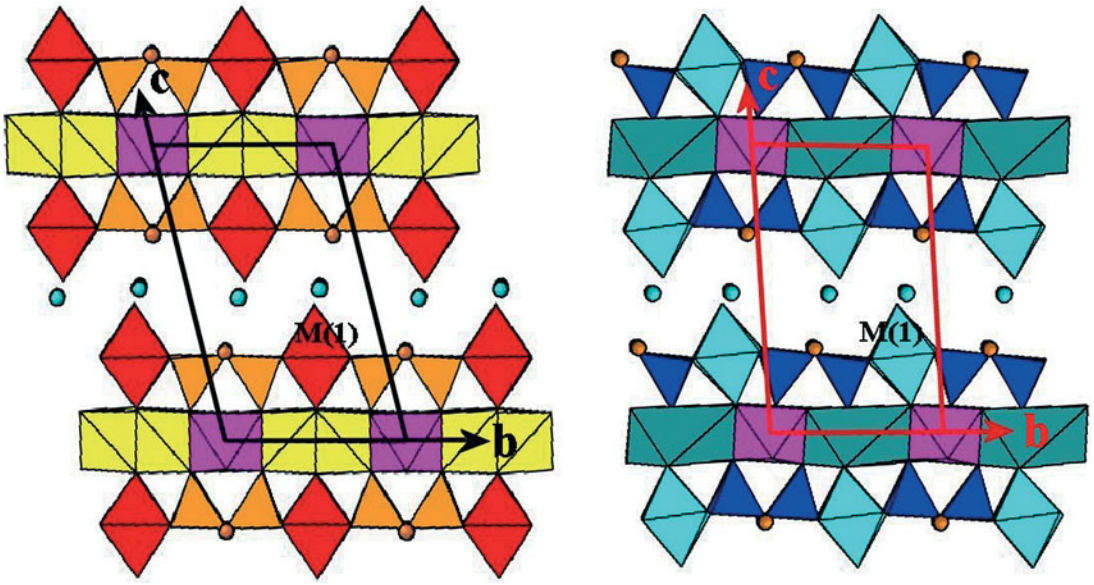

FIG. 5. Projection along [100] of the crystal structures of epistolite (left side) and murmanite (right side). The red and pale blue *M*(1) octahedra occurring in the heteropolyhedral *H* sheet are dominated by Nb and Ti in epistolite and murmanite, respectively. In the *O* sheet of octahedra, the fuchsia octahedra are centered on Ti; the blue and yellow octahedra contain Na. The interlayer content corresponds to Na (orange filled circles) and H_2O (blue filled circles).

Structural formulae

In the literature, the following compositional data are available for epistolite and murmanite. These data are to be compared with the formulae obtained from our measurements (Table 2) and given above.

Epistolite: $Na_{1.73}\{(Na_{1.29}Ti_{1.45}Ca_{0.47}Fe^{3+}_{0.07}Mn_{0.17}Mg_{0.20}Nb_{0.19}K_{0.16})_{\Sigma 4}[Nb_2O_4(Si_{3.94}Al_{0.06})_{\Sigma 4}O_{14}]((OH)_{1.08}F_{0.68}(H_2O)_{0.24})_{\Sigma 2}\}\bullet 5.765H_2O$ (Semenov *et al.* 1962; H_2O by DTA); $Na_{1.12}\{(Na_{2.63}Ti_{0.96}Ca_{0.27}K_{0.05}Fe^{3+}_{0.04}Mn_{0.04}Ta_{0.01})_{\Sigma 4}[(Nb_{1.92}Ti_{0.08})_{\Sigma 2}(O_2(H_2O)_2)_{\Sigma 4}Si_4O_{14}](OH_{1.10}F_{0.55}O_{0.35})_{\Sigma 2}\}\bullet 2.19H_2O$ (Sokolova & Hawthorne 2004; H_2O by structural analysis).

Murmanite: $Na_{0.27}\{(Na_{1.57}Ti_{1.32}Ca_{0.32}Fe^{3+}_{0.38}Mn_{0.25}Mg_{0.16})_{\Sigma 4}[(Ti_{1.51}Nb_{0.32}Zr_{0.17})_{\Sigma 4}(O_2(OH)_2)_{\Sigma 4}Si_4O_{14}]((H_2O)_{1.96}(OH)_{0.04})_{\Sigma 2}\}\bullet 1.63H_2O$ (Semenov *et al.* 1962; H_2O by DTA); $Na_{0.48}\{(Na_{1.28}Ti_{1.54}Ca_{0.76}Fe^{2+}_{0.18}Fe^{3+}_{0.06}Mn_{0.08}K_{0.04}Mg_{0.06})_{\Sigma 4}[(Ti_{1.72}Nb_{0.28})_{\Sigma 2}(O_2(H_2O)_2)_{\Sigma 2}Si_4O_{14}](O_{1.29}H_2O_{0.71})_{\Sigma 2}\}\bullet 1.04H_2O$ (Karup-Møller 1986a; H_2O by difference of electron-microprobe data from 100%).

The available chemical data support a deficiency of interlayer cations both in epistolite and murmanite, a result confirmed by our structural analyses and, for epistolite, by that of Sokolova & Hawthorne (2004). In the formulae given above, only Na is considered as an interlayer cation, mainly because it is not easy to prove that other cations [*e.g.*, Ca as indicated by Sokolova & Hawthorne (2004)] are located there. According to the ideal structure, the content of both Na and H_2O could reach a maximum of two units per formula unit (*upfu*). The H_2O content of epistolite and murmanite has been analytically determined only by Semenov *et al.* (1962), but their value for epistolite is clearly overestimated. Other estimates of H_2O in the two minerals are derived as a difference of the electron-microprobe results from to 100% (for which caution must be observed) and, for epistolite, by structural analysis (Sokolova & Hawthorne 2004). Overall, the content of interlayer H_2O seems to be close to two *upfu* in both minerals. In conclusion, we are in favor of the following ideal formulae: $(Na,\square)_2\{(Na,Ti)_4[Nb_2(O,H_2O)_4Si_4O_{14}](OH,F)_2\}\bullet 2H_2O$ for epistolite and $(Na,\square)_2\{(Na,Ti)_4[Ti_2(O,H_2O)_4Si_4O_{14}](OH,F)_2\}\bullet 2H_2O$ for murmanite.

Both minerals have an interlayer content represented by Na, H_2O and vacancies. As repeatedly reported in literature, the main difference they show is in the content of the *M*(1) octahedron (*Z* cation): Ti predominates over Nb in epistolite and *vice versa* for murmanite. In both minerals, Ti occurs also in the *O* sheet; the Na:Ti ratio is higher in epistolite than in murmanite, with a trend toward 3:1 and 1:1, respectively. In a broad sense, epistolite and murmanite differ from their parent phase, vuonnemite and epistolite (Table 1), respectively, by the interlayer content only, as expected for transforma-

tion minerals on the basis of the inheritance principle mentioned above. In the primary phases, in fact, the interlayer includes PO_4 groups and more Na, but no H_2O. That fact is reflected in the *c* parameter, which is substantially longer in vuonnemite (*a* 5.49, *b* 7.16, *c* 14.42 Å, α 92.57, β 95.28, γ 90.58°) and lomonosovite (*a* 5.39, *b* 7.12, *c* 14.45 Å, α 99.72, β 96.43, γ 90.28°) than in the secondary phases epistolite and murmanite (Table 3) derived from them. The values of the unit-cell parameters of vuonnemite and lomonosovite are taken from Nèmeth (2004).

Reticular basis supporting syntaxy between epistolite and shkatulkalite

Experimental observations prove that in our samples, epistolite forms a syntaxy with some proportion of shkatulkalite. In spite of the difference in the *c* parameters of the two phases, most of the nodes in their weighted reciprocal lattices (*i.e.*, spots of the diffraction patterns) overlap exactly or nearly so owing to the existence of a pseudo-orthorhombic supercell in common to the two minerals, as given below.

The triclinic *P* cell of epistolite (Table 3) is transformed to a pseudomonoclinic *B*-centered supercell (*a* 5.455, *b* 7.160, *c* 46.923 Å, α 93.13, β 90.57, γ 90.03°) by the matrix |$\bar{1}$ 0 0||0 $\bar{1}$ 0||1 2 4| and to a pseudo-orthorhombic *A*-centered supercell (*a* 5.455, *b* 7.160, *c* 93.728 Å, α 88.75, β 90.57, γ 90.03°) by the matrix |$\bar{1}$ 0 0||0 $\bar{1}$ 0||2 3 8|.

The monoclinic *P* cell of shkatulkalite [*a* 5.468, *b* 7.18, *c* 15.55 Å, β 94.0°; modified from that of Men'shikov *et al.* (1996) as explained earlier] is transformed to a monoclinic *P* supercell (*a* 5.468, *b* 7.18, *c* 46.589 Å, β 92.72°) by the matrix |$\bar{1}$ 0 0||0 $\bar{1}$ 0||1 0 3| and to a pseudo-orthorhombic *B*-centered supercell (*a* 5.468, *b* 7.18, *c* 93.079 Å, β 89.36°) by the matrix |$\bar{1}$ 0 0||0 $\bar{1}$ 0||1 0 6|.

The matrices needed to transform the indices of epistolite to those of shkatulkalite and *vice versa* are |1 0 0||0 $\bar{1}$ 0||–1/2 –1/2 –4/3| and |1 0 0||0 $\bar{1}$ 0||–3/8 3/8 –3/4|, respectively. Thus a diffraction spot of epis-

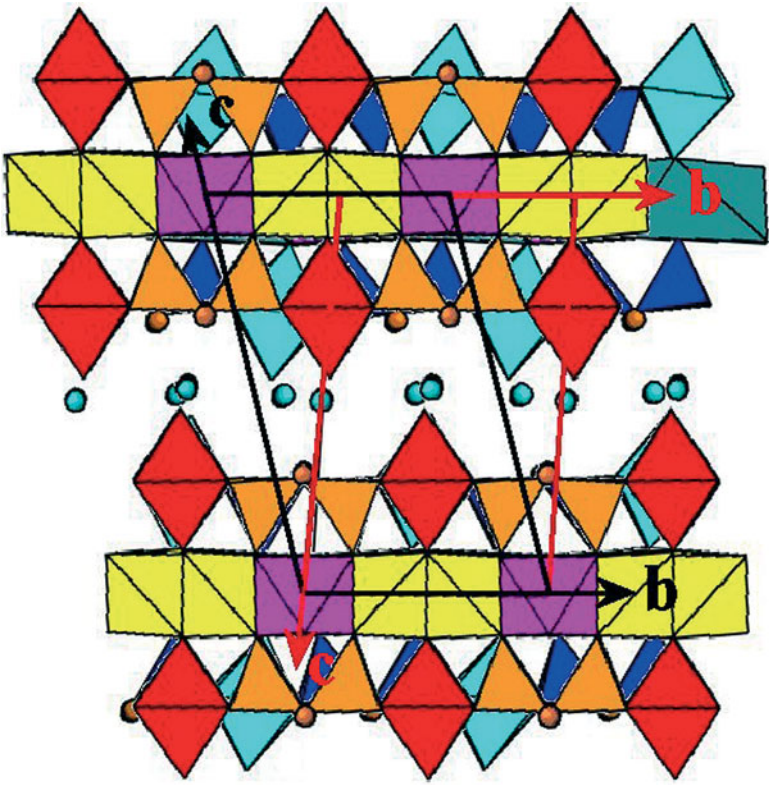

FIG. 6. Projection along [100] of the superimposed structures of epistolite and murmanite (for orientation, see text). The common origin of the reference system is fixed on the Ti atom of the *O* sheet; this position is not a center of symmetry in murmanite. Colors as in Figure 5.

tolite exactly overlaps one of shkatulkalite if $-(3h + 3k + 8l) = 6n$ (n integer); *i.e.*, 1/6 of the whole diffraction-pattern exactly overlaps. Besides, as shown by Figure 7, most of the not-exactly-overlapping spots of one phase are very close to a spot of the other phase.

Reticular basis supporting syntaxy between epistolite and murmanite

At first sight, the unit cells of epistolite and murmanite differ sufficiently in their angles (Table 3) to expect only an occasional overlap of nodes in a common reciprocal space. However, the two minerals share at least two supercells that support the syntaxy found experimentally. Specifically, the triclinic *P* cell of murmanite (Table 3) is transformed to the following two supercells that match those given above for epistolite: 1) a monoclinic *P* supercell (*a* 5.387, *b* 7.079, *c* 46.524 Å, α 93.84, β 91.34, γ 90.00°) by the matrix |1 0 0||0 1 0||1 0 4|, and 2) a pseudo-orthorhombic *A*-centered supercell (*a* 5.387, *b* 7.079, *c* 92.843 Å, α 89.47, β 91.35, γ 90.01°) by the matrix |1 0 0| |0 1 0||2 1 8|.

The same matrix |1 0 0||0 1 0||–1/2 –1/2 $\bar{1}$| transforms the indices of the diffraction spots of epistolite to those of murmanite and *vice versa*. Thus all spots of epistolite and murmanite with the same parity of *h* and *k*, *i.e.*, half of the whole set of spots, exactly overlap each other. Besides, for the half set of spots that does not exactly overlap, close vicinity between spots belonging to different phases is invariably observed (Fig. 8).

Reticular basis supporting possible twinning in epistolite and murmanite

The layer titanosilicates listed in Table 1 have in common a two-dimensional cell *ab* ~5.4 × 7.0 Å (or multiples) corresponding to the periodicity observed in the *HOH* layer. As noted by Ferraris & Nèmeth (2003) and further discussed by Ferraris *et al*. (2004), for most of these compounds, the value of the third periodicity and of the β angle is such that the relation $c\sin(\beta - 90) \cong a/n$ (n = 3, 4, ...) holds. This relation implies that a row [*uvw*] with periodicity $c_o \cong nc\sin\beta$ and normal to the *ab* plane does exist. The supercell with parameters *a*, *b* and c_o is (pseudo)orthorhombic if α = 90° (monoclinic members) and (pseudo)monoclinic (angle $\alpha_m \cong$ 90°) in the triclinic members with γ ≅ 90°. Besides the pseudomonoclinic and pseudo-orthorhombic supercells given above for epistolite and murmanite, the latter allows also a smaller pseudomonoclinic *P* supercell with *a* 5.387, *b* 7.079, *c* 34.887 Å, α 93.84, β 89.13, γ 90.00° obtained from the basic cell of Table 3 by the matrix |$\bar{1}$ 0 0||0 $\bar{1}$ 0||$\bar{1}$ 0 $\bar{3}$|.

The occurrence of supercells with higher symmetry favors twinning (Ferraris *et al*. 2004); thus on the basis of the monoclinic supercells given above, {100} twinning by reticular pseudomerohedry can be expected in epistolite and murmanite. Further, {010} and {001} twinning can be expected also because of the reported pseudo-orthorhombic supercells. The presence of twinning by reticular merohedry may in principle be revealed by the occurrence of systematic non-space-group absences [see an example referred to the layer titanosilicates in Ferraris *et al*. (2004)]. However, the complex diffraction-pattern caused by the presence of syntaxy of epistolite with murmanite (plus other phases, as discussed above) can obscure the splitting of spots and systematic non-space-group absences expected in some types of twinning. Consequently, because of the plurality of effects related to various kinds of oriented domains, no clear signs of twinning have been detected in our crystals of epistolite and murmanite, even if the phenomenon cannot be excluded.

Conclusions

The analysis of electron and X-ray diffraction patterns, together with evidence gathered in the refinement of the crystal structures, show that, at least for our samples, the obstacles to properly refine the structures of epistolite and murmanite are mainly due to the widespread presence of syntaxy between these two layer heterophyllosilicates. Intergrowth of other heterophyllosilicates, like shkatulkalite, disorder at various scales, like polytypism and easy {001} cleavage, and likely twinning, further affect the diffracted intensities. In the literature, (i) the overlap of diffraction patterns contributed by different domains and (ii) the presence of weak superstructure reflections, presumably due to cation ordering, has even led to proposals of different unit-cells for these minerals, *e.g.*, the cell with double *a* and *b* used by Rastsvetaeva & Andrianov (1986) for murmanite. The non-reduced cell (*a* 5.38, *b* 7.05, *c* 12.17 Å, α 93.16, β 107.82, γ 90.06°) given by Khalilov (1989) for murmanite can instead be converted into the corresponding conventional cell (*a* 5.38, *b* 7.05, *c* 11.70 Å, α 86.69, β 81.87, γ 89.94°) by the transformation |$\bar{1}$ 0 0||0 1 0||$\bar{1}$ 0 $\bar{1}$|.

Now that it has been made clear by Sokolova & Hawthorne (2004) that murmanite and epistolite are not isostructural, evidence that these minerals (plus shkatulkalite?) are derived, respectively, from the primary phases lomonosovite and vuonnemite by hydration and loss of PO_4 agrees even more with the inheritance principle of Khomyakov (1995). In fact, the two pairs of one primary and one secondary phase have a different topology of the *HOH* layer that is preserved through the transformation lomonosovite → murmanite and vuonnemite → epistolite. In principle, one could expect a shkatulkalite-like phase derived from lomonosovite, but evidence for this hypothetical phase has not been detected. Semenov *et al*. (1962) have instead reported a different secondary phase accompanying murmanite and called it "metamurmanite". This phase has been detected in our sample of murmanite too, but cannot be

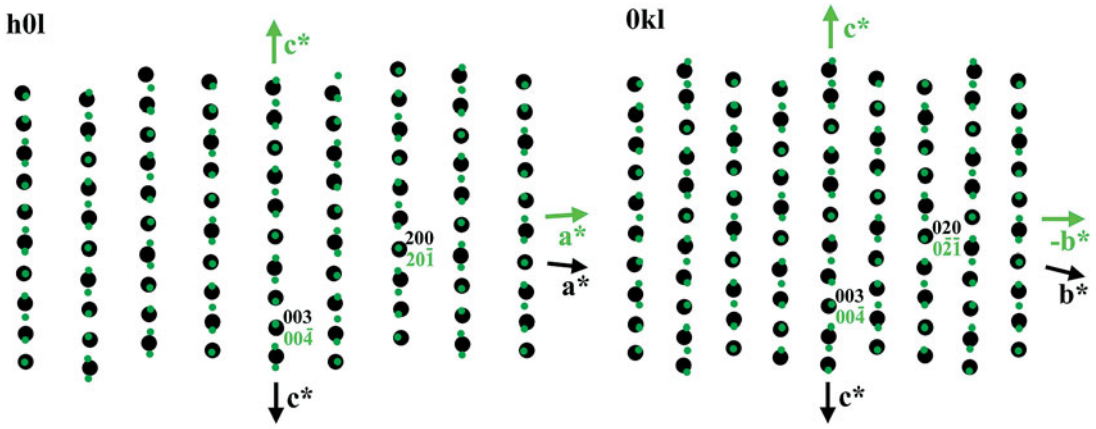

FIG. 7. Superimposed *h0l* (left side) and 0*kl* planes (right side) of the reciprocal lattices of epistolite (black dots) and shkatulkalite (green dots). See text for conditions of exact overlap.

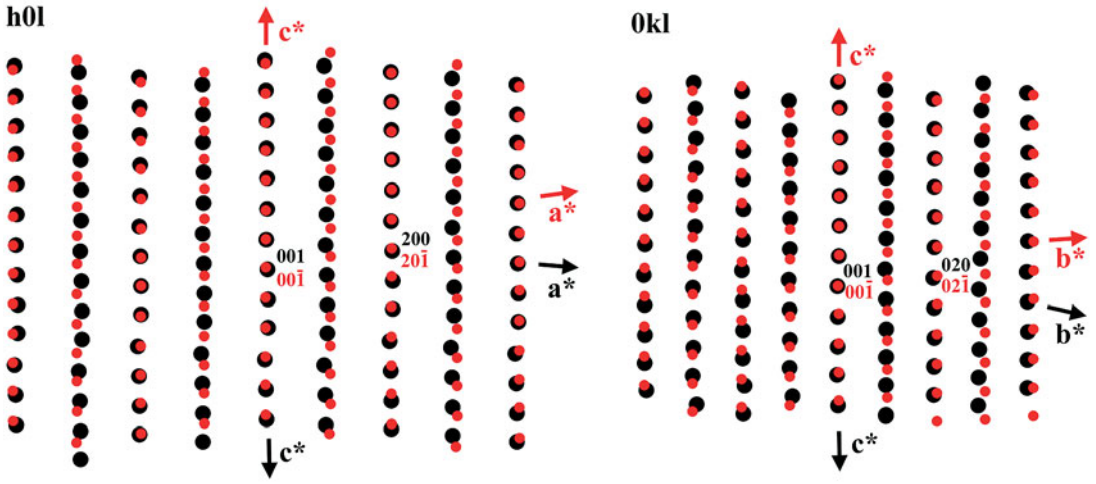

FIG. 8. Superimposed *h0l* (left side) and 0*kl* planes (right side) of the reciprocal lattices of epistolite (black dots) and murmanite (red dots). Exact overlap is observed where, in both lattices, either *h* or *k* is even.

better characterized. Presumably, the different topology of the *HOH* layer in lomonosovite and murmanite favors a different path of transformation.

Intergrowths between the two primary minerals vuonnemite and lomonosovite have been observed also (Pekov 2000; I.V. Pekov, pers. commun.). The high R value of the structure refinement (14% for lomonosovite; Belov *et al*. 1978) and the same short M(1)–O distances (about 1.8 Å) described above for epistolite and murmanite that occur even in low-R structure refinement (R = 1.8% for vuonnemite; Ercit *et al*. 1998), are signs of a possible syntaxy between vuonnemite and lomonosovite. The even worse situation found in refining the structures of epistolite and murmanite might be related to an increase of disorder in the secondary phases.

The different topology of the *HOH* layer in epistolite and murmanite, in spite of their close chemical composition, is likely related to the Na:Ti ratio in the *O* sheet and the type of *Z* cation. An oxygen atom shared by an *H* and *O* sheet is bonded to four cations, three belonging to the *O* sheet and one to the *H* sheet. Because of bond-valence balance, even an O^{2-} anion cannot be bonded only to high-charge cations like Si^{4+} and Ti^{4+} or Nb^{5+}; consequently, constraints are applied not only to the composition, but also to the topology of the *HOH* layer.

Thus, to reach a suitable bond-valence balance, Na octahedra share edges between them in epistolite, but not in murmanite (Fig. 5), and a different connectivity between the *H* and *O* sheets is established.

Acknowledgements

We are grateful to I.V. Pekov for communicating some field observations on the association of minerals here described, to G. Artioli and I. Sajo for help in collecting X-ray powder-diffraction patterns, to S. Bigi for assistance in chemical analyses, to referee E. Sokolova, whose harsh criticism helped us to detect some weak points in the original version, and to the editor R.F. Martin, who, as usual, improved linguistically and scientifically the text. G.F. acknowledges financial support by MIUR (PRIN and FIRB grants) and CNR (instrument facilities at Università di Torino and Università di Modena e Reggio Emilia). P.N. benefitted from a doctorate grant of the Università di Torino. O.A.A. is grateful to B. Borutzky, M. Sokolova and Z. Shlukova for providing samples.

References

Bellezza, M., Franzini, M., Larsen, A.O., Merlino, S. & Perchiazzi, N. (2004): Grenmarite, a new member of the götzenite – seidozerite – rosenbuschite group from the Langesundsfjord district, Norway: definition and crystal structure. *Eur. J. Mineral.* **16**, 971-978.

Belov, N.V., Gavrilova, G.S., Solovieva, L.P. & Khalilov, A.D. (1978): The refined structure of lomonosovite. *Sov. Phys. Dokl.* **22**, 422-424.

Bøggild, O.B. (1901): Epistolite, a new mineral. *Medd. Grønland* **24**, 183-190.

Burke, E.A.J. & Ferraris, G. (2004): New minerals and nomenclature modifications approved in 2003 by the Commission on New Minerals and Mineral Names, International Mineralogical Association. *Can. Mineral.* **42**, 905-913.

Buchwald, V. & Sørensen, H. (1961): An autoradiographic examination of rocks and minerals from the Ilímaussaq batholith, south-west Greenland. *Medd. Grønland* **162**, 1-35.

Chernov, A.N, Ilyukhin, V.V., Maksimov B.A. & Belov, N.V. (1971): Crystal structure of innelite, Na_2Ba_3(Ba,K,Mn)(Ca,Na)Ti$(TiO_2)_2[Si_2O_7]_2(SO_4)_2$. *Sov. Phys. Crystallogr.* **16**, 65-69.

Christiansen, C.C., Johnsen, O. & Makovicky, E. (2003): Crystal chemistry of the rosenbuschite group. *Can. Mineral.* **41**, 1203-1224.

_____, Makovicky, E. & Johnsen, O.N. (1999): Homology and typism in heterophyllosilicates: an alternative approach. *Neues Jahrb. Mineral., Abh.* **175**, 153-189.

Egorov-Tismenko, Yu.K. & Sokolova, E.V. (1990): Structural mineralogy of the homologic series seidozerite–nacaphite. *Mineral. Zh.* **12**(4), 40-49 (in Russ.).

Ercit, T.S., Cooper, M.A. & Hawthorne, F.C. (1998): The crystal structure of vuonnemite, $Na_{11}Ti^{4+}Nb_2(Si_2O_7)_2(PO_4)_2O_3$(F,OH), a phosphate-bearing sorosilicate of the lomonosovite group. *Can. Mineral.* **36**, 1311-1320.

Ferraris, G. (1997): Polysomatism as a tool for correlating properties and structure. *In* Modular Aspects of Minerals (S. Merlino, ed.). *Eur. Mineral. Union, Notes in Mineralogy* **1**, 275-295.

_____, Belluso, E., Gula, A., Soboleva, S.V., Ageeva, O.A. & Borutskii, B.E. (2001a): A structural model of the layer titanosilicate bornemanite based on seidozerite and lomonosovite modules. *Can. Mineral.* **39**, 1665-1673.

_____ & Gula, A. (2005): Polysomatic aspects of microporous minerals – heterophyllosilicates, palysepioles and rhodesite-related structures. *Rev. Mineral. Geochem.* **57**, 69-104.

_____, Ivaldi, G., Khomyakov, A.P., Soboleva, S.V., Belluso, E. & Pavese, A. (1996): Nafertisite, a layer titanosilicate member of a polysomatic series including mica. *Eur. J. Mineral.* **8**, 241-249.

_____, _____, Pushcharovsky, D.Yu., Zubkova, N. & Pekov, I.V. (2001b): The crystal structure of delindeite, $Ba_2\{(Na,K,\square)_3(Ti,Fe)[Ti_2(O,OH)_4Si_4O_{14}](H_2O,OH)_2\}$, a member of the mero-plesiotype bafertisite series. *Can. Mineral.* **39**, 1307-1316.

_____, Makovicky, E. & Merlino, S. (2004): *Crystallography of Modular Materials*. IUCr/Oxford University Press, Oxford, U.K.

_____ & Nèmeth, P. (2003): Pseudo-symmetry, twinning and structural disorder in layer titanosilicates. *ECM–21* (*Durban*), *Abstr.*, 41.

Guan, Ya.S., Simonov, V.I. & Belov, N.V. (1963): Crystal structure of bafertisite, $BaFe_2TiO[Si_2O_7](OH)_2$. *Dokl. Acad. Sci. USSR, Earth-Sci. Sect.* **149**,123-126 (published 1965).

Gutkova, N.N. (1930): A new titano-silicate – murmanite from Lovozero tundras. *Dokl. Akad. Nauk SSSR, ser. A*, 731-736 (in Russ.).

Hong, Wenxing & Fu, Pingqiu (1982): Jinshajiangite – a new Ba–Mn–Fe–Ti-bearing silicate mineral. *Geochemistry* (*China*) **1**, 458-464 (in Chinese).

Karup-Møller S. (1986a): Murmanite from the Ilímaussaq alkaline complex, South Greenland. *Neues Jahrb. Mineral., Abh.* **155**, 67-88.

_____ (1986b): Epistolite from Ilímaussaq alkaline complex in South Greenland. *Neues Jahrb. Mineral., Abh.* **155**, 289-304.

KHALILOV, A.P. (1989): Refinement of the crystal structure of murmanite and new data on its crystal chemistry. *Mineral. Zh.* **11**(5), 19-27 (in Russ.).

_____, MAMEDOV, K.S., MAKAROV, YE.S. & P'YANZINA, L.YA. (1965): Crystal structure of murmanite. *Dokl. Akad. Nauk SSSR* **161**, 150-152 (in Russ.).

KHOMYAKOV, A.P. (1995): *Mineralogy of Hyperagpaitic Alkaline Rocks*. Clarendon Press, Oxford, U.K.

MAKOVICKY, E. (1997): Modularity – different types and approaches. *In* Modular Aspects of Minerals (S. Merlino, ed.). *Eur. Mineral. Union, Notes in Mineralogy* **1**, 315-344.

MATSUBARA, S. (1980): The crystal structure of orthoericssonite. *Mineral. J.* **10**, 107-121.

MCDONALD, A.M., GRICE, J.D. & CHAO, G.Y. (2000): The crystal structure of yoshimuraite, a layered Ba–Mn–Ti silicophosphate, with comments of five-coordinated Ti^{4+}. *Can. Mineral.* **38**, 649-656.

MEN'SHIKOV, YU.P., KHOMYAKOV, A.P., POLEZHAEVA, L.I. & RASTSVETAEVA, R.K. (1996): Shkatulkalite: $Na_{10}Mn_4Ti_3Nb_3(Si_2O_7)_6(OH)_2F{\bullet}12H_2O$ – a new mineral. *Zap. Vser. Mineral. Obshchest.* **125**(1), 120-126 (in Russ.).

MOORE, P.B. (1971): Ericssonite and orthoericssonite. Two new members of the lamprophyllite group, from Långban, Sweden. *Lithos* **4**, 137-145.

NÈMETH, P. (2004): *Characterization of New Mineral Phases Belonging to the Heterophyllosilicate Series*. Ph.D. dissertation, Università di Torino, Torino, Italy.

PEKOV, I.V. (2000): *Lovozero Massif: History, Pegmatites, Minerals*. Ocean Pictures Ltd, Moscow, Russia.

_____ & CHUKANOV, N.V. (2005): Microporous framework silicate minerals with rare, and transition elements: minerogenetic aspects. *Rev. Mineral. Geochem.* **57**, 145-172.

PENG, ZHIZHONG, ZHANG, JIANHONG & SHU, JINFU (1984): The crystal structure of barytolamprophyllite and orthorhombic lamprophyllite. *Kexue Tongbao* **29**, 237-241.

PUSHCHAROVSKY, D.YU., PASERO, M., MERLINO, S., VLADYKIN, N.V., ZUBKOVA, N.V. & GOBECHIYA, E.R. (2002): Crystal structure of zirconium-rich seidozerite. *Crystallogr. Rep.* **47**, 196-200.

PUTNIS, A. (2002): Mineral replacement reactions: from macroscopic observations to microscopic mechanisms. *Mineral. Mag.* **66**, 689-708.

RAMSAY, W. (1890): Geologische Beobachtungen auf der Halbinsel Kola. Nebst einem Anhange: petrographische Beschreibung der Gesteine des Lujavr-urt. *Fennia* **3**, 1-52.

RASTSVETAEVA, R.K. (1998): Crystal structure of betalomonosovite from the Lovozero region. *Sov. Phys. Crystallogr.* **31**, 633-636.

_____ & ANDRIANOV, V.I. (1986): New data on the crystal structure of murmanite. *Sov. Phys. Crystallogr.* **31**, 44-48.

_____ & CHUKANOV, N.V. (1999): Crystal structure of a new high-barium analogue of lamprophyllite with a primitive unit cell. *Dokl. Chem.* **368**(4-6), 228-231.

_____, SOKOLOVA, M.N. & GUSEV, A.I. (1990): Refined crystal structure of lamprophyllite. *Mineral. Zh.* **12**(5), 25-28 (in Russ.).

_____, TAMAZYAN, R.A., SOKOLOVA, E.V. & BELAKOVSKII, D.I. (1991): Crystal structures of two modifications of natural Ba,Mn-titanosilicate. *Sov. Phys. Crystallogr.* **36**, 186-189.

ROZENBERG, K.A., RASTSVETAEVA, R.K. & VERIN, I.A. (2003): Crystal structure of surkhobite: new mineral from the family of titanosilicate micas. *Crystallogr. Rep.* **48**, 384-389.

SEMENOV, E.I., ORGANOVA, N.I. & KUKHARCHIK, M.V. (1962): New data on minerals of the lomonosovite–murmanite group. *Sov. Phys. Crystallogr.* **6**, 746-751.

SHANNON, R.D. (1976): Revised effective ionic radii and systematic studies of interatomic distances in halides and chalcogenides. *Acta Crystallogr.* **A32**, 751-767.

SOKOLOVA, E.V., EGOROV-TISMENKO, YU.K. & KHOMYAKOV, A.P. (1987): Special features of the crystal structure of $Na_{14}CaMgTi_4[Si_2O_7]_2[PO_4]_2O_4F_2$ – homologue of sulphohalite and lomonosovite structure types. *Mineral. Zh.* **9**(3), 28-35 (in Russ.).

_____, _____ & _____ (1988): Crystal structure of sobolevite. *Sov. Phys. Dokl.* **33**, 711-714.

_____ & HAWTHORNE, F.C. (2001): The crystal chemistry of the $[M_3\phi_{11-14}]$ trimeric structures from hyperagpaitic complexes to saline lakes. *Can. Mineral.* **39**, 1275-1294.

_____ & _____ (2004): The crystal chemistry of epistolite. *Can. Mineral.* **42**, 797-806.

UNGEMACH, H. (1935): Sur la syntaxie et la polytypie. *Z. Kristallogr.* **91**, 1-22.

YAMNOVA, N.A., EGOROV-TISMENKO, YU.K. & PEKOV, I.V. (1998): Crystal structure of perraultite from the Coastal Region of the Sea of Azov. *Crystallogr. Rep.* **43**, 401-410.

ZHOU, H., RASTSVETAEVA, R.K., KHOMYAKOV, A.P., MA, Z. & SHI, N. (2002): Crystal structure of new micalike titanosilicate – bussenite, $Na_2Ba_2Fe^{2+}[TiSi_2O_7][CO_3]O(OH)(H_2O)$. *Crystallogr. Rep.* **47**, 43-46.

Received July 26, 2004, revised manuscript accepted May 2, 2005.